# Tumor Growth Modeling via Fokker-Planck Equation

Hossein Heidari[1], Mahdi Rezaei Karamati[1], Hossein Motavalli[1]

*Department of Theoretical and Astrophysics, Faculty of Physics, University of Tabriz, Tabriz, Iran*

**Abstract**

In the present investigation, a stochastic tumor growth model is presented based on the Morse potential. The solution of the Fokker-Planck equation is used to study the growth rate and the geometry of breast cancer with and without radiation therapy effects. In the second case, to estimate unknown parameters of the probability density function, breast data from the Surveillance, Epidemiology, and End Results program and machine learning algorithm are used. By considering three groups of women (35-85 years old), the results show that as time goes on, tumor size increases while its growth rate decreases, and the older women have a slower growth rate. Also, the simulation results of breast tumors of mice confirm that our results are consistent with the experimental evidence in both cases of radiotherapy and no treatment. Finally, the finding of this study implies that the present model is accurate than the Gompertz one in predicting tumor size, in the treatment case.

*Keywords:* `Tumor growth, Fokker-Planck equation, Morse potential, Breast cancer, Stochastic phenomena, Mathematical model`

## 1. Introduction

Cancer is a complicated process, which occurs by a mutation in Germ-line and Soma [1]. Successful treatment depends on the timely diagnosis and selection of appropriate therapy. In recent decades, mathematical models have been used to understand the mechanism, selecting appropriate therapy [2], and find new methods of treatment [3]. Scientists and physicians are very inter-

ested in predicting the geometry and growth rate of the tumor, where they can play a considerable role in choosing a treatment with less harmful effects[4, 5]. Mathematical models of tumor growth were proposed as exponential and non-exponential [6]. In the earliest studies on cancer, it was supposed that the tumor grows exponentially fast and unlimited [7], while subsequent studies showed that the growth rate is fast, but as the tumor size gets larger, its growth rate becomes slower than exponential [8, 9, 10]. Generally, non-exponential models are classified as deterministic and stochastic. Biological phenomena such as tumors are affected by random events, so they have a random nature. Therefore, tumor growth and its geometry are different from predictions of deterministic models [11, 12]. Some models, such as power-law, logistic, Allee, hyperbolastic, and Gompertz is used as non-exponential. Some of these models have been used as both deterministic and stochastic. Some examples of stochastic models include the study of tumor invasion to healthy tissue in hybrid models [13], investigation of the growth in primary breast cancer by using the power law [14], and the study of the malignant growth in the early phase of the tumor by the Allee model [15]. Among these models, Gompertz and logistic are so popular. Gompertz model was first used by Laird to describe tumor growth [16], and widely used in the reviews of literature such as [11, 17] or is considered as a stochastic model with [18, 19, 20, 21] and without the effects of therapy[22]. Also, logistics [23] and modified logistic [24] models, are some examples of logistic growth that are used for the investigation of the cancer cell population.

Biological systems such as tumors are affected by many external and internal influences. These influences are often called noise or fluctuations and are not fully known. Furthermore, to treat these systems exactly, one has to solve the equations of motion for each particle of the system. But such systems have a large number of particles that make it impossible. Alternatively, one can use a stochastic description of macroscopic variables that fluctuate randomly. One of the simplest equations of motion for the distribution function of fluctuating macroscopic variables is the Fokker-Planck equation (FPE) [25]. This equation has been widely used to model biological phenomena such as tumor growth

[18, 19, 20, 21, 22, 23, 24, 25, 26]. The FPE, in most cases, cannot be solved analytically [25]. Some methods, such as Nikiforov–Uvarov [27], analogy with the Schrödinger equation [28, 29, 30, 31], Fourier Spectral [32], and differential transform methods [33] have been used to solve this equation. In analogy with the Schrödinger equation, one may use some similarity transformations and the change of variables to transform FPE to the Schrödinger-like equation [34]. The solution of the FPE depends on the diffusion function and interaction potential. Mathematical models may include unknown parameters that can be estimated by machine learning algorithms, such as particle swarm optimization algorithm (PSO) [35].

In this paper, we propose a FPE model to describe tumor growth by physical Morse potential, in the framework of a stochastic phenomenon. To investigate tumor growth, the solution of the FPE is obtained. Then, by using the PSO algorithm, unknown parameters are estimated and, the growth rate of mouse and human breast cancer with and without radiation therapy effects is studied. This paper is organized as follows: In section 2, for Morse potential and a specific diffusion function, the probability density function (PDF) of FPE is obtained. Then, tumor growth in breast cancer is discussed by comparing the results of our model with experimental data, in section 3. Finally, section 4 remarks the conclusions.

## 2. The Solution of the Fokker-Planck Equation

FPE is one of the most popular differential equations which can describe non-equilibrium systems in physics, chemistry, biology, and circuit theory [25]. This equation, mathematically, is a linear partial differential equation, which is used to describe stochastic systems and the Brownian motion of particles. By considering the tumor growth as a stochastic phenomenon, the one-dimensional FPE of the probability density distribution, $P(x;t)$, of the tumor size is given by

$$\frac{\partial}{\partial t}P(x,t) = \frac{\partial^2}{\partial x^2}(D(x,t)P(x,t)) - \frac{\partial}{\partial x}(f(x,t)P(x,t)), \tag{1}$$

where, $D(x,t)$ and $f(x,t)$ are diffusion function and drift force, respectively. Depending on the mathematical form of these functions, the resulting equation may be highly complicated or relatively simple, and accordingly, numerical algorithms or analytical solutions are proposed. Among various methods suggested in the literature, transformation to the Schrödinger equation is one of the most common approaches. In this formalism, each pair of drift and diffusion coefficients in FPE corresponds to a potential or Hamiltonian in the non-relativistic quantum mechanics. One may assume that $D(x,t)$ and $f(x,t)$ are associated with the position, without any dependence on time. In this framework, for the evolutionary process of tumor growth, based on Albano and Giorno's model [18], we suppose a quadratic form for diffusion function as follows

$$D(x) = D_0 x^2, \tag{2}$$

where $x$ is tumor size, and $D_0$ indicates a parameter related to the environmental properties. Moreover, following commonly used mathematical models which are widely used in biology [36, 37, 38, 39], we assume that cancer growth is affected by the Morse potential,

$$V_{eff}(y) = A\left(e^{-2ay} - 2e^{-ay}\right), \tag{3}$$

where $y = \frac{1}{\sqrt{D_0}} Ln(x)$ is an auxiliary variable, and $A$ and $a$ are positive constants related to the depth and width of potential, respectively. The existence of equivalence between FP and Schrödinger equations, allows one to obtain drift force by using (2) and (3) functions as follows (see appendix A and B)

$$\begin{aligned} f(x) = \frac{1}{cW_{k,0}\left(\frac{2k}{x}\right) + M_{k,0}\left(\frac{2k}{x}\right)} \Bigg[ & 2D_0 cx W_{k+1,0}\left(\frac{2k}{x}\right) \\ & + \sqrt{D_0}\Bigg(\left(2\sqrt{D_0}cx + 2\sqrt{A}cx - 2\sqrt{A}c\right) W_{k,0}\left(\frac{2k}{x}\right) \\ & - \left(\sqrt{D_0}x + 2\sqrt{A}x\right) M_{k+1,0}\left(\frac{2k}{x}\right) \\ & + \left(2\sqrt{D_0}x + 2\sqrt{A}x - 2\sqrt{A}\right) M_{k,0}\left(\frac{2k}{x}\right)\Bigg)\Bigg], \end{aligned} \tag{4}$$

where, $W_{\nu,\mu}(z)$ and $M_{\nu,\mu}(z)$ are Whittaker functions, $c$ is a constant, and $k = \sqrt{\frac{A}{D_0}}$.

Furthermore, one may describe the solution of Eq. (1) by using the transition probability density $p(x, x_0; t)$ as $P(x,t) = \int p(x, x_0; t)P(x_0, t_0)dx_0$, in which zero-index variables refer to the initial conditions. By combining these, the solution of Eq. (1) can be written as [28]

$$p(x, x_0; t) = \zeta(x, x_0)K(x, x_0; t), \tag{5}$$

where (see appendix A and B)

$$\zeta(x, x_0) = x^{\frac{3}{2}} e^{-\frac{1}{2D_0}\int_{x_0}^{x} \frac{f(x)}{x^2} dx}, \tag{6}$$

and

$$K(x, x_0, t) = \frac{a(xx_0)^{\frac{1}{2}}}{4\pi^2} \int_0^\infty \alpha e^{\frac{-a^2\alpha^2}{8}t} \sinh(\pi\alpha) \left|\Gamma(i\alpha)\right|^2 \times W_{\frac{1}{2},\frac{i\alpha}{2}}(\frac{1}{x_0}) W_{\frac{1}{2},\frac{i\alpha}{2}}(\frac{1}{x}) d\alpha. \tag{7}$$

In the next section, we will use the obtained PDF (Eq. 5) to predict the tumor growth rate and its geometry.

## 3. Results and Discussion

Due to the random behavior of tumor growth and the many parameters which affect the properties of the tumor, FPE is an appropriate model to describe this stochastic phenomenon. The PDF obtained for Morse's potential can be used to describe tumor growth, such as breast tumor. This function has some parameters, such as $D_0$, that can be determined using machine learning algorithms. For this purpose, we used the PSO algorithm, which is based on some animals such as the bird's (particles) flocks movement to find food. In this algorithm, each particle is used to search for the solution to the problem, and the particle system is initialized with a population of random solution parameters [40]. In addition, the position of particle $i$, in search space, is denoted by $x_i^k$ at iteration $k$, and particles have a memory so that their best position is called $p$. Also, the overall best location value obtained, so far, by any particle

in the population is called $g$. Accordingly, the position of each particle at each iteration is given by

$$x_i^{k+1} = x_i^k + v_i^{k+1}, \tag{8}$$

where $v_i^k$ is a velocity of particle $i$ that moves in the search space and is updated as

$$v_i^{k+1} = w * v_i^k + c_1 * rand * (p_i^k - x_i^k) + c_2 * rand * (g_i^k - x_i^k), \tag{9}$$

where $w$ is inertia weight, $c_1$ and $c_2$ are learning factors. In the following, we focus on the growth rate of the breast tumor by using the PDF and PSO algorithm mentioned above.

### *3.1.* ***Growth Rate without Treatment***

To investigate the growth rate without treatment, we used the experimental data for the PSO algorithm, from the Surveillance, Epidemiology, and End Results (SEER) program [41], which provides information on cancer statistics in various locations of the United States according to several components such as race, sex, and age. Here, tumor data were gathered from multiple sources from 1973 up to the present. To find the time evolution of the PDF, one needs to have at least two data sets at different times, but there is not more than one set. In general, the treatment process should be started a few days after the primary tumor diagnosis, which can affect the control parameters. For this purpose, researchers usually use tumor volume doubling time (DT), that is, the period that the volume of the tumor is doubled. Here, the DT calculated by Peer et al. [42] is used to find the time evolution of PDF. It was calculated for three age groups: 80 days for group I (women younger than 49 years), 157 days for group II (women between 50-69 years), and 188 days for group III (women older than 69 years). Furthermore, we studied linear growth, in the sense that, the tumor size data are presented as the mean diameter in SEER. Meanwhile, the PSO algorithm was run 11 times for each group ( consisting of 3655, 8867, and 6097 persons for groups I, II, and III, respectively). Based on the above assumption, the estimated parameters are given in Table 1.

Table 1: The evaluated potential and diffusion parameters

| *Group* | *Age Range* | $D_0$ $(1/year)$ | $a$ $(1/\sqrt{year})$ | $A$ $(ev)$ | $c$ |
|---|---|---|---|---|---|
| I | 35-49 | 0.56 | 0.75±0.03 | 1.58 | -0.50±0.02 |
| II | 50-69 | 0.32 | 0.57±0.01 | 0.90 | -0.77±0.04 |
| III | 70-85 | 0.28 | 0.53±0.01 | 0.79 | -0.92±0.08 |

According to table 1, $D_0$, $a$, $A$, and $c$ are decreased by increasing age. Also, the behavior of the PDF is shown in Fig. (5) for three groups.

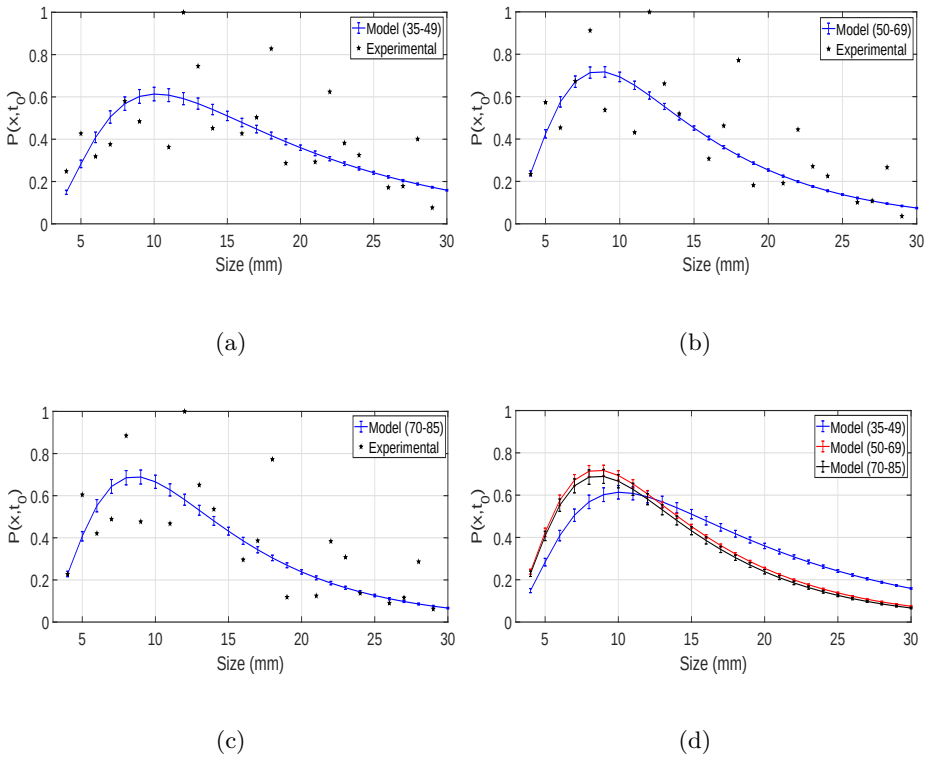


Figure 1: The PDF of the breast cancer interms of the tumor size: (a) group I with $A = 1.58\ ev$, $a = 0.75\ 1/\sqrt{year}$, $D_0 = 0.56\ 1/year$, $c = -0.50$, (b) group II with $A = 0.90\ ev$, $a = 0.57\ 1/\sqrt{year}$, $D_0 = 0.32\ 1/year$, $c = -0.77$, (c) group III with $A = 0.79\ ev$, $a = 0.53\ 1/\sqrt{year}$, $D_0 = 0.28\ 1/year$, $c = -0.92$, (d) comparison between the three groups.

Accordingly, the highest probability of tumor size occurs in the range of 7–

11 $mm$. Additionally, as the age decreases, the maximum value of probability decreases and it is shifted to a greater size. Before surgery [43] or other therapeutic methods, predicting the tumor size and its geometry can be important. Here, we estimated tumor size using the PDF for three age groups, which are indicated in Fig. (2). Accordingly, the growth rate of the tumor size decreases as age goes up. Consequently, the young women group has a faster growth rate than the older one, which is consistent with the other studies, such as [42]. Also, the growth rate goes slower by increasing time. Experimental results and mathematical models show that the growth rate decreases (because of factors such as limited nutrition) with the increasing tumor boundaries [12, 24, 44], which verify our results. Moreover, the behavior of Morse potential for triple groups, according to Eq. (3), is shown in Fig. (3). It can be seen that the potential for group I is deeper than that of the other groups, which is in agreement with Fig. 2 with faster growth for this group. Equivalently, according to Fig. (5) PDF of young women is bigger than older women for the large size of the tumor.

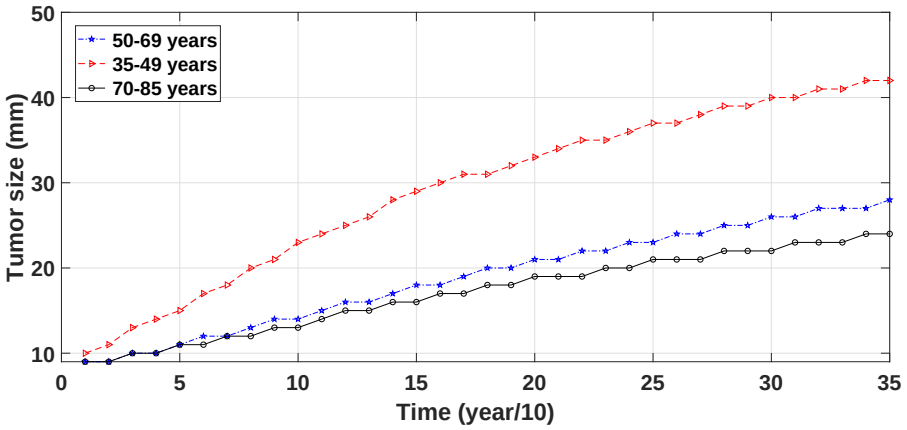


Figure 2: Comparison of the time evolution of the tumor size for three groups.

For further confirmation, one may compare the present model with a popular model such as the Gompertz model, where its drift force is given by

$$f(x) = \alpha x - \beta x \ln(x), \tag{10}$$

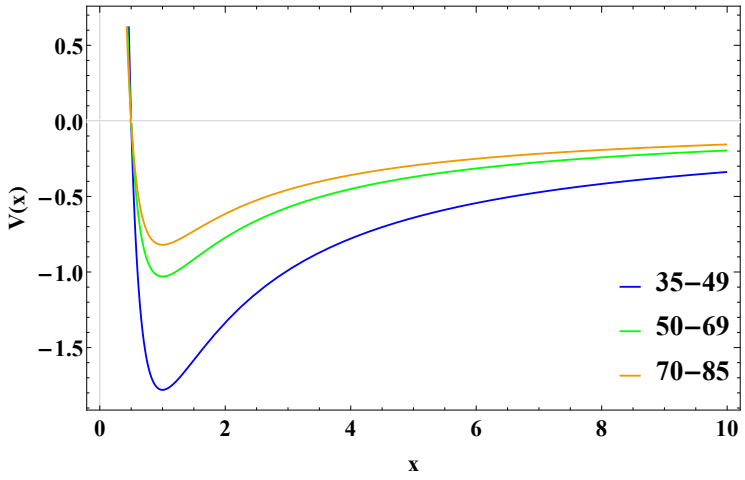


Figure 3: The evaluated potential V(x) versus the tumor size x. The different age groups are indicated in the figure.

in which $x$ indicates tumor size, $\alpha$ and $\beta$ are cell's birth and mortality rates parameters, respectively. To fit these parameters, we have used the PSO algorithm and experimental data for three age groups, in the same manner as our model.

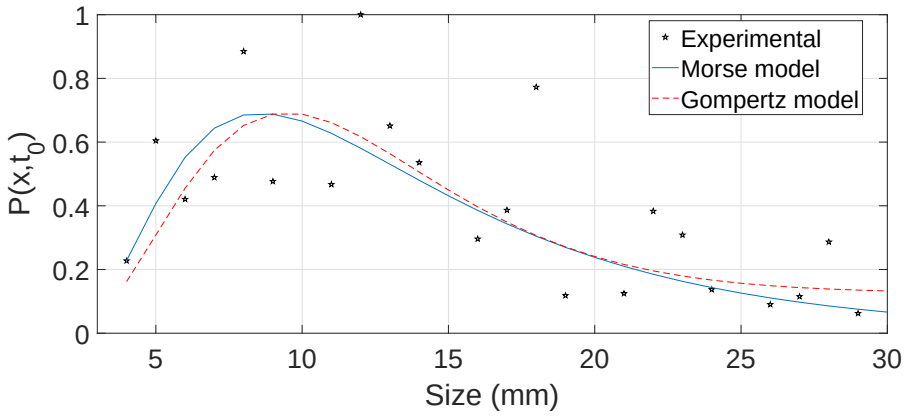


Figure 4: The mean PDF of the Gompertz (dashed line) and Morse (solid line) models in terms of tumor size for the group III, with MSE value 0.034 for both models. The Gompertz model parameters are $\alpha = 4.62$, $\beta = 1.69$, $D0 = 0.55$.

The results of the two models are presented in Fig. (4), and a comparison between them indicates that the Mean Square Error (MSE) value of the two models is equal to 0.034. Consequently, the accuracies of the two models are similar in this case.

### *3.2.* ***Growth Rate with Radiotherapy***

In order to consider treatment, we used the breast data taken from [45], where the effects of radiotherapy were studied on breast tumors in mice. The tumor was exposed to 6 Gy radiation therapy and its volume was measured every 3 days. Also, the initial tumor size was $2.27mm$ before radiotherapy. By applying the same method which was used in the absence of therapy in the previous section, and using these data as well as the PSO algorithm, we can estimate the model parameters and mean value of tumor size. The estimated parameters are given in Tables 2 and 3.

Table 2: The evaluated Morse model parameters

| | $D_0$ $(1/day)$ | $a$ $(1/\sqrt{day})$ | $A$ $(ev)$ | $c$ |
|---|---|---|---|---|
| $Nontreated$ | 0.21 | 0.46 | 2.9 | 3.5 |
| $Rdiotherapy$ | 0.15 | 0.39 | 1.9 | 3.9 |

Table 3: The evaluated Gompertz model parameters

| | $\alpha$ | $\beta$ | $\sigma$ |
|---|---|---|---|
| $Nontreated$ | 0.83 | 0.30 | 0.39 |
| $Rdiotherapy$ | 1.49 | 0.09 | 0.72 |

According to the Table 2, radiotherapy reduced all model parameters except the $c$.

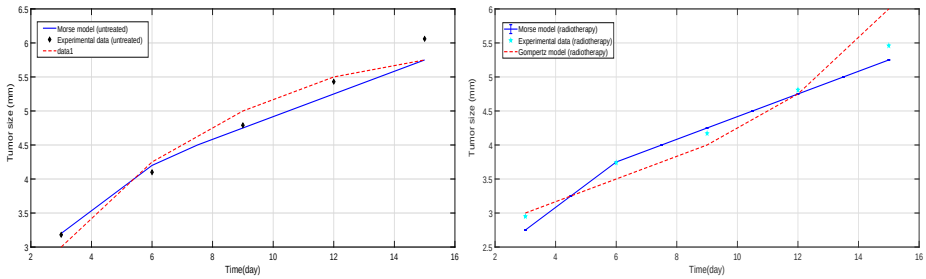


(a) (b)

Figure 5: Time evolution of the mean breast tumor size: (a) for the Morse and Gompertz models before therapy with MSE=0.032 and MSE=0.033, respectively and, (b) for the Morse and Gompertz models after therapy with MSE=0.019 and MSE=0.077, respectively.

The simulation results are shown in Fig. 5(a) and Fig. 5(b) for untreated and treated cases, respectively. The solid and dashed lines represent the Morse and Gompertz models predictions, respectively. A comparison between them indicates that the MSE values of the Gompertz are more than Morse. Obviously, the high value of MSE denotes low accuracy in tumor growth prediction. This implies that the Morse model is accurate than the Gompertz one, and therefore, can be used to estimate tumor size evolution over time, in the treatment case.

## 4. Conclusions

We have proposed a stochastic model for tumor growth based on FPE for a quadratic diffusion function and Morse potential. To verify the accuracy of the proposed model, the growth rate of breast cancer was considered with and without radiation therapy effects. In the absence of therapy, simulations showed that as the mean size of the tumor is going to be bigger, its growth becomes slower; meanwhile, younger women experience faster growth rates than the older one. Furthermore, in the presence of therapy, the results show that

the proposed model is in good agreement with those taken from experimental data. Specifically, our model is accurate than the Gompertz one, and therefore, is suitable for estimating the time evolution of tumor size, in the treatment case.

## 5. Acknowledgments

We are grateful to Dr. Mojtaba Karimi Habil for his valuable comments. This paper is published as a part of a research project supported by the Iran National Science Foundation (No. 96001905).

## References

[1] R. A. Weinberg, R. A. Weinberg, The biology of cancer, Vol. 1, Garland science New York, 2007.

[2] A. M. Austin, M. J. Douglass, G. T. Nguyen, S. N. Penfold, A radiobiological markov simulation tool for aiding decision making in proton therapy referral, Physica Medica 44 (2017) 72–82.

[3] D. Sigal, M. Przedborski, D. Sivaloganathan, M. Kohandel, Mathematical modelling of cancer stem cell-targeted immunotherapy, Mathematical Biosciences 318 (2019) 108269.

[4] L. Tang, A. L. Van De Ven, D. Guo, V. Andasari, V. Cristini, K. C. Li, X. Zhou, Computational modeling of 3d tumor growth and angiogenesis for chemotherapy evaluation, PloS one 9 (1) (2014) e83962.

[5] Y. Liu, T. C. Chan, C.-G. Lee, Y.-B. Cho, M. K. Islam, A stochastic model for tumor geometry evolution during radiation therapy in cervical cancer, Medical physics 41 (2) (2014) 021705.

[6] E. Mehrara, E. Forssell-Aronsson, H. Ahlman, P. Bernhardt, Specific growth rate versus doubling time for quantitative characterization of tumor growth rate, Cancer research 67 (8) (2007) 3970–3975.

[7] P. Gerlee, The model muddle: in search of tumor growth laws, Cancer research 73 (8) (2013) 2407–2411.

[8] W. V. Mayneord, On a law of growth of jensen's rat sarcoma, The American Journal of Cancer 16 (4) (1932) 841–846.

[9] A. Brú, S. Albertos, J. L. Subiza, J. L. García-Asenjo, I. Brú, The universal dynamics of tumor growth, Biophysical journal 85 (5) (2003) 2948–2961.

[10] L. Norton, Cancer stem cells, self-seeding, and decremented exponential growth: theoretical and clinical implications, Breast disease 29 (1) (2008) 27–36.

[11] F. B. Hanson, C. Tier, A stochastic model of tumor growth, Mathematical Biosciences 61 (1) (1982) 73–100.

[12] R. Wette, I. Katz, E. Rodin, Stochastic processes for solid tumor kinetics i. surface-regulated growth, Mathematical Biosciences 19 (3-4) (1974) 231–255.

[13] A. R. Anderson, A hybrid mathematical model of solid tumour invasion: the importance of cell adhesion, Mathematical medicine and biology: a journal of the IMA 22 (2) (2005) 163–186.

[14] D. Hart, E. Shochat, Z. Agur, The growth law of primary breast cancer as inferred from mammography screening trials data, British journal of cancer 78 (3) (1998) 382.

[15] Y. Liang, R. Yang, Y. Guo, C. Jiang, L. Liu, Y. Wan, Y. Shao, Spatiotemporal dynamics of different growth-diffusion systems on a percolation lattice, Phys. Rev. E 99 (2019) 042401.

[16] A. K. Laird, Dynamics of tumour growth, British journal of cancer 18 (3) (1964) 490.

[17] L. Norton, A gompertzian model of human breast cancer growth, Cancer research 48 (24 Part 1) (1988) 7067–7071.

[18] G. Albano, V. Giorno, A stochastic model in tumor growth, Journal of Theoretical Biology 242 (2) (2006) 329–336.

[19] G. Albano, V. Giorno, P. Román-Román, F. Torres-Ruiz, Inferring the effect of therapy on tumors showing stochastic gompertzian growth, Journal of Theoretical Biology 276 (1) (2011) 67–77.

[20] G. Albano, V. Giorno, P. Román-Román, S. Román-Román, F. Torres-Ruiz, Estimating and determining the effect of a therapy on tumor dynamics by means of a modified gompertz diffusion process, Journal of theoretical biology 364 (2015) 206–219.

[21] G. Albano, V. Giorno, P. Román-Román, S. Román-Román, J. Serrano-Pérez, F. Torres-Ruiz, Inference on an heteroscedastic gompertz tumor growth model, Mathematical Biosciences 328 (2020) 108428.

[22] C.-F. Lo, A modified stochastic gompertz model for tumour cell growth, Computational and Mathematical Methods in Medicine 11 (1) (2010) 3–11.

[23] B.-Q. Ai, X.-J. Wang, G.-T. Liu, L.-G. Liu, Correlated noise in a logistic growth model, Physical Review E 67 (2) (2003) 022903.

[24] T. Bose, S. Trimper, Stochastic model for tumor growth with immunization, Physical Review E 79 (5) (2009) 051903.

[25] H. Risken, The fokker-planck equation. methods of solution and applications, vol. 18 of, Springer series in synergetics 301 (1989).

[26] C. Lo, Exact solution of the functional fokker–planck equation for cell growth with asymmetric cell division, Physica A: Statistical Mechanics and its Applications 533 (2019) 122079.

[27] H. Heidari, H. Motavalli, M. R. Keramati, Exact solutions of fokker–planck equation via the nikiforov–uvarov method, Indian Journal of Physics (2020) 1–7.

[28] A. Okopińska, Fokker-planck equation for bistable potential in the optimized expansion, Physical Review E 65 (6) (2002) 062101.

[29] G. Borges, E. Drigo Filho, R. Ricotta, Variational supersymmetric approach to evaluate fokker–planck probability, Physica A: Statistical Mechanics and its Applications 389 (18) (2010) 3892–3899.

[30] R. Anjos, G. Freitas, C. Coimbra-Araújo, Analytical solutions of the fokker–planck equation for generalized morse and hulthén potentials, Journal of Statistical Physics 162 (2) (2016) 387–396.

[31] M. Araujo, E. Drigo Filho, A general solution of the fokker-planck equation, Journal of Statistical Physics 146 (3) (2012) 610–619.

[32] A. S. Polunchenko, G. Sokolov, An analytic expression for the distribution of the generalized shiryaev–roberts diffusion, Methodology and Computing in Applied Probability 18 (4) (2016) 1153–1195.

[33] S. Hesam, A. Nazemi, A. Haghbin, Analytical solution for the fokker–planck equation by differential transform method, Scientia Iranica 19 (4) (2012) 1140–1145.

[34] A. Gonzalez-Lopez, N. Kamran, P. J. Olver, Normalizability of one-dimensional quasi-exactly solvable schrödinger operators, Communications in mathematical physics 153 (1) (1993) 117–146.

[35] A. T. Kiani, M. F. Nadeem, A. Ahmed, I. A. Sajjad, M. S. Haris, L. Martirano, Optimal parameter estimation of solar cell using simulated annealing inertia weight particle swarm optimization (saiw-pso), in: 2020 IEEE International Conference on Environment and Electrical Engineering and 2020 IEEE Industrial and Commercial Power Systems Europe (EEEIC/I&CPS Europe), IEEE, 2020, pp. 1–6.

[36] M. Peyrard, A. R. Bishop, Statistical mechanics of a nonlinear model for dna denaturation, Physical review letters 62 (23) (1989) 2755.

[37] H. Choi, H. Kang, H. Park, Extended morse function model for angle-dependent hydrogen bond in protein- protein interactions, The Journal of Physical Chemistry B 114 (8) (2010) 2980–2987.

[38] M. Hillebrand, G. Kalosakas, A. Schwellnus, C. Skokos, Heterogeneity and chaos in the peyrard-bishop-dauxois dna model, Physical Review E 99 (2) (2019) 022213.

[39] M. R. Duff Jr, J. M. Borreguero, M. J. Cuneo, A. Ramanathan, J. He, G. Kamath, S. C. Chennubhotla, F. Meilleur, E. E. Howell, K. W. Herwig, et al., Modulating enzyme activity by altering protein dynamics with solvent, Biochemistry 57 (29) (2018) 4263–4275.

[40] R. Eberhart, J. Kennedy, A new optimizer using particle swarm theory, in: MHS'95. Proceedings of the Sixth International Symposium on Micro Machine and Human Science, Ieee, 1995, pp. 39–43.

[41] Surveillance, epidemiology, and end results (seer) program (www.seer.cancer.gov) seer*stat database: Incidence - seer 18 regs research data + hurricane katrina impacted louisiana cases, nov 2017 sub (1973-2015 varying) - linked to county attributes - total u.s., 1969-2016 counties, national cancer institute, dccps, surveillance research program, released april 2018, based on the november 2017 submission.

[42] P. G. Peer, J. A. Van Dijck, A. L. Verbeek, J. H. Hendriks, R. Holland, Age-dependent growth rate of primary breast cancer, Cancer 71 (11) (1993) 3547–3551.

[43] K. Nakashima, T. Uematsu, K. Takahashi, S. Nishimura, Y. Tadokoro, T. Hayashi, T. Sugino, Does breast cancer growth rate really depend on tumor subtype? measurement of tumor doubling time using serial ultrasonography between diagnosis and surgery, Breast Cancer 26 (2) (2019) 206–214.

[44] H. Enderling, M. AJ Chaplain, Mathematical modeling of tumor growth and treatment, Current pharmaceutical design 20 (30) (2014) 4934–4940.

[45] A. Kefayat, F. Ghahremani, H. Motaghi, M. A. Mehrgardi, Investigation of different targeting decorations effect on the radiosensitizing efficacy of albumin-stabilized gold nanoparticles for breast cancer radiation therapy, European Journal of Pharmaceutical Sciences 130 (2019) 225–233.

[46] W. Fischer, H. Leschke, P. Muller, Changing dimension and time: two well-founded and practical techniques for path integration in quantum physics, Journal of Physics A: Mathematical and General 25 (13) (1992) 3835.

[47] M. Abramowitz, I. A. Stegun, Handbook of mathematical functions: with formulas, graphs, and mathematical tables, Vol. 55, Courier Corporation, 1965.

## Appendix A: Solution of the Quasi-Exactly Solvable Schrödinger Equation

Generally, the FPE is not analytically solvable except for a limited number of drift and diffusion functions [28, 31, 30]. For the PDF, $P(x,t)$, one may write the FPE in the form of quasi-exactly solvable Schrödinger equation as

$$-T(t)P(x,t) = P_1(x)\frac{\partial^2}{\partial x^2}P(x,t) + P_2(x)\frac{\partial}{\partial x}P(x,t) + R(x)P(x,t), \qquad (11)$$

where $T(t)$, $P_1(x)$, $P_2(x)$, and $R(x)$ are time- and position-dependent operators. An appropriate method to solve this equation is a Hamiltonian formalism, in the framework of non-relativistic quantum mechanics. For time-independent drift force, $f(x)$, and diffusion function, $D(x)$, we use separation variables method as

$$P(x,t) = \Psi(x)\xi(t), \qquad (12)$$

which leads to eigenfunction equation $L_{QS}\Psi(x) = -\lambda\Psi(x)$ with

$$L_{QS} = P_1(x)\frac{d^2}{dx^2} + P_2(x)\frac{d}{dx} + R(x), \qquad (13)$$

and $\xi(t) = e^{-\lambda t}$, in which $\lambda$ is an eigenvalue. By introducing the auxiliary variable $y = \int \frac{dx}{\sqrt{P_1(x)}}$, Eq. (11) is transformed into

$$-T = \frac{d^2}{dy^2} + h(y)\frac{d}{dy} + R(y), \tag{14}$$

where $h(y) = \frac{1}{\sqrt{p_1}}(p_2 - \frac{1}{2\sqrt{p_1}}\frac{dp_1}{dy})$. Now, let us introduce a similarity transformation as $\Psi_n(y) = \zeta(y)^{-1}\varphi_n(y)$, which allows one to write related Hamiltonian as

$$-H = \frac{d^2}{dy^2} + (h - 2\frac{\zeta'}{\zeta})\frac{d}{dy} + (R - \frac{\zeta''}{\zeta} + 2\frac{\zeta}{\zeta^2}^{\prime 2} - h\frac{\zeta'}{\zeta}), \tag{15}$$

where primes denote the derivatives with respect to $y$. In order to transform equation (15) to the Schrödinger one, the coefficient of the first-order derivative must be equal to zero

$$h - 2\frac{\zeta'}{\zeta} = 0. \tag{16}$$

According to this choice, $\zeta(y)^{-1}$ is given by

$$\zeta(y)^{-1} = e^{-\frac{1}{2}\int \frac{1}{\sqrt{p_1}}(p_2 - \frac{1}{2\sqrt{p_1}}\frac{dp_1}{dy})dy}. \tag{17}$$

Consequently, the quasi-exactly solvable Schrödinger equation takes the following form

$$-\frac{d^2}{dy^2}\varphi_n(y) + V_{eff}(y)\varphi_n(y) = E_n\varphi_n(y), \tag{18}$$

where $E_n$ is energy eigenvalue and $V_{eff}(y)$ indicates effective potential as

$$V_{eff}(y) = -R + \frac{1}{2}\frac{d}{dy}(\frac{p_2}{\sqrt{p_1}} - \frac{1}{2p_1}\frac{dp_1}{dy}) + \frac{1}{4p_1}(p_2 - \frac{1}{2\sqrt{p_1}}\frac{dp_1}{dy})^2. \tag{19}$$

Now, by taking into account $p(x,t|x_0,t_0)$ and $K(x,t|x_0,t_0)$ as Green's functions of $P(x,t)$ and Schrödinger equation, respectively, one gets [28]

$$p(x,x_0;t) = \zeta(x,x_0)^{-1}K(x,x_0;t), \tag{20}$$

where, $p(x,x_0;t) = p(x,t|x_0,t_0=0)$ and $K(x,x_0;t) = K(x,t|x_0,t_0=0)$.

## Appendix B: Solution of the FPE for Morse Potential

The general form of the one-dimensional FPE for the PDF, $P(x,t)$, is

$$\frac{\partial}{\partial t}P(x,t) = \frac{\partial^2}{\partial x^2}(D(x,t)P(x,t)) - \frac{\partial}{\partial x}(f(x,t)P(x,t)), \tag{21}$$

where $D(x,t)$ and $f(x,t)$ are diffusion and drift functions respectively, which both are related to interaction potential in the Schrödinger equation. PDF in the Eq. (21) can be described by the transition probability density (TPD), $p(x,x_0;t)$, as $P(x,t) = \int p(x,x_0;t)P(x_0,t_0)dx_0$, in which zero-index variables represent the initial conditions. By assuming $D(x) = D_0x^2$, Eq. (21) becomes

$$\frac{\partial}{\partial t}P(x,t) = D_0x^2\frac{\partial^2 P(x,t)}{\partial x^2} + (4D_0x - f(x))\frac{\partial P(x,t)}{\partial x} + (2D_0 - \frac{\partial f(x)}{\partial x})P(x,t), \tag{22}$$

Comparing Eq. (22) and Eq. (11), leads to

$$\begin{aligned} p_1(x) &= D_0x^2 \\ p_2(x) &= 4D_0x - f(x) \\ R(x) &= 2D_0 - \tfrac{\partial f(x)}{\partial x}. \end{aligned} \tag{23}$$

By inserting (23) into (19) and (17) one gets

$$V_{eff}(x) = \frac{1}{2}\frac{df}{dx} - \frac{f}{x} + \frac{f^2}{4D_0x^2} + \frac{1}{4}D_0, \tag{24}$$

$$\zeta(x,x_0)^{-1} = x^{-\frac{3}{2}}e^{\frac{1}{2D_0}\int_{x_0}^{x}\frac{f(x)}{x^2}dx}. \tag{25}$$

Now, by comparing effective potential (22) with the Morse potential

$$V(y) = A\left(e^{-2ay} - 2e^{-ay}\right), \tag{26}$$

we obtain the following nonlinear first order differential equation for drift function

$$x^2\frac{df}{dx} + \frac{f^2}{2D_0} - 2xf + \frac{D_0}{2}x^2 + 4Ax - 2A = 0, \tag{27}$$

with $D_0 = a^2$. Solution of Eq. 27 is given by

$$f(x) = \frac{1}{cW_{k,0}\left(\frac{2k}{x}\right) + M_{k,0}\left(\frac{2k}{x}\right)}\Bigg[2D_0 cx W_{k+1,0}\left(\frac{2k}{x}\right) + \sqrt{D_0}\Bigg(\left(2\sqrt{D_0}cx + 2\sqrt{A}cx - 2\sqrt{A}c\right)W_{k,0}\left(\frac{2k}{x}\right) - \left(\sqrt{D_0}x + 2\sqrt{A}x\right)M_{k+1,0}\left(\frac{2k}{x}\right) + \left(2\sqrt{D_0}x + 2\sqrt{A}x - 2\sqrt{A}\right)M_{k,0}\left(\frac{2k}{x}\right)\Bigg)\Bigg], \quad (28)$$

where $W_{\nu,\mu}(z)$ and $M_{\nu,\mu}(z)$ are Whittaker functions and $k = \sqrt{\frac{A}{D_0}}$. Now, it is necessary to find out the time-dependent Morse Green function, $K(x, x_0; t)$, which its energy-dependent defined as follow [46]

$$G(x, x_0; p) = \frac{2(xx_0)^{\frac{1}{2}}\Gamma(\frac{\nu}{2} - \frac{\omega}{2} + \frac{1}{2})}{a\omega\Gamma(\nu + 1)} \times W_{\frac{\omega}{2},\frac{\nu}{2}}(\frac{\omega}{x_0})M_{\frac{\omega}{2},\frac{\nu}{2}}(\frac{\omega}{x}), \quad (29)$$

where $p = -E > 0$ also

$$\omega = \frac{2}{a}\sqrt{2A}, \qquad \nu = \frac{2}{a}\sqrt{2p}. \quad (30)$$

Now, one can obtain $K(x, x_0; t)$ by using the inverse Laplace transformation of (29) as

$$K(x, x_0; t) = \lim_{T\to\infty} \frac{1}{2\pi i}\int_{\gamma - iT}^{\gamma + iT} e^{pt}G(x, x_0; p)dp. \quad (31)$$

To solve this integral, we use the residue theorem and consider the counter-clockwise simple closed curve $C$ in Fig. 6, as

$$\oint_C e^{pt}G(x, x_0; p)dp = 2\pi i \sum residue, \quad (32)$$

where the residues associated with singularities which lie inside the contour $C$. Green function (29) has two types of singularities, first is related to the Gamma function, $\Gamma(\frac{\nu}{2} - \frac{\omega}{2} + \frac{1}{2})$, where singularities are obtained by setting $\frac{\nu}{2} - \frac{\omega}{2} + \frac{1}{2} = -n$, therefore,

$$p_n = \frac{a^2}{8}\left(\omega - 2n - 1\right)^2, \quad n = 0, 1, ... \quad (33)$$

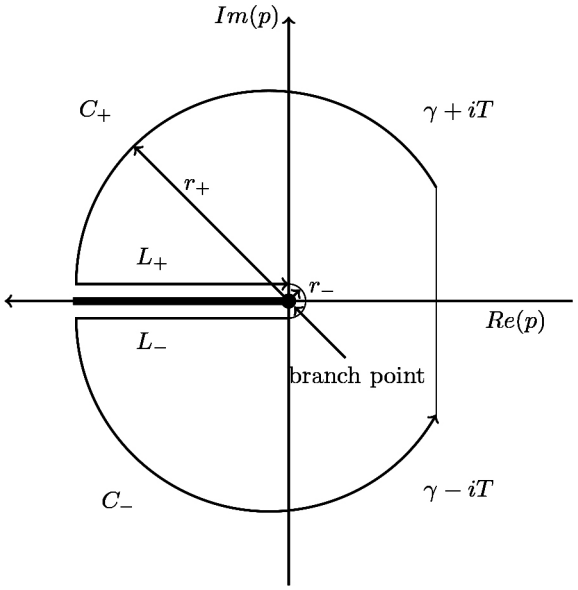


Figure 6: counterclockwise simple closed curve $C$

The second type of singularity is related to the square root of $p$ in relation (30), which introduces a branch cut in the range $(0, -\infty)$. According to Fig. 6, the integral over $C$ is written as

$$\begin{aligned}\oint_C e^{pt}G(x,x_0;p)dp = &\int_{C_+} e^{pt}G(x,x_0;p)dp \\ &+ \int_{L_+} e^{pt}G(x,x_0;p)dp + \int_{L_-} e^{pt}G(x,x_0;p)dp \\ &+ \int_{C_-} e^{pt}G(x,x_0;p)dp + \int_{\gamma-iT}^{\gamma+iT} e^{pt}G(x,x_0;p)dp. \quad (34)\end{aligned}$$

As $t$ approaches infinity, the PDF should be finite, so it requires $p = 0$ and $\omega = 1$. But $p = 0$ is a branch point, so there are not any poles in the $C$, which implies that $\sum residue = 0$. Since $W_{\frac{\omega}{2},\frac{\nu}{2}}(\frac{\omega}{x_0})$ and $\frac{M_{\frac{\omega}{2},\frac{\nu}{2}}(\frac{\omega}{x})}{\Gamma(\nu+1)}$ are analytical functions inside of the counter $C$, integrals along the arcs $C_+$ and $C_-$ equal to zero, as $r_+ \to \infty$ and $r_- \to 0$. Therefore time-dependent Green function, $K(x, x_0; t)$, reduces to

$$K(x,x_0;t) = -\lim_{T\to\infty} \frac{1}{2\pi i}\left[\int_{L_+} e^{pt}G(x,x_0;p)dp + \int_{L_-} e^{pt}G(x,x_0;p)dp\right]. \quad (35)$$

To calculate the integrals along segments $L_+$ and $L_-$, branch cut is needed to parameterize as the form $-\nu^2 = \alpha^2$, where $\alpha \in [0, T]$ as $T \to \infty$. So $K(x, x_0; t)$ is written in terms of new variable as

$$K(x,x_0;t) = \frac{a^2}{8\pi i}\left[\int_{\infty}^{0} G(x,x_0;i\alpha)e^{-\frac{a^2}{8}\alpha^2 t}d\alpha + \int_{0}^{\infty} G(x,x_0;-i\alpha)e^{-\frac{a^2}{8}\alpha^2 t}d\alpha\right]. \tag{36}$$

Substituting $G$ in Eq. (35) and using $W_{\nu,\mu}(z) = W_{\nu,-\mu}(z)$ one obtains

$$\begin{aligned} K(x,x_0;t) = -\frac{a(xx_0)^{\frac{1}{2}}}{4\pi i}\int_0^{\infty} \alpha e^{-\frac{a^2}{8}\alpha^2 t} W_{\frac{1}{2},i\frac{\alpha}{2}}(\frac{1}{x_0}) \\ \times\left(\frac{\Gamma(i\frac{\alpha}{2})}{\Gamma(i\alpha+1)}M_{\frac{1}{2},i\frac{\alpha}{2}}(\frac{1}{x}) - \frac{\Gamma(-i\frac{\alpha}{2})}{\Gamma(-i\alpha+1)}M_{\frac{1}{2},-i\frac{\alpha}{2}}(\frac{1}{x})\right)d\alpha. \end{aligned} \tag{37}$$

The Whittaker function $W_{a,b}(z)$ is related to $M_{a,b}(z)$ through

$$W_{a,b}(z) = \frac{\Gamma(2b)}{\Gamma(\frac{1}{2}-b-a)}M_{a,b}(z) + \frac{\Gamma(2b)}{\Gamma(\frac{1}{2}+b-a)}M_{a,-b}(z). \tag{38}$$

By using the properties of gamma functions (page 256, Relations 6.1.15 and 6.1.29 [47]) and (38), we can write the explicit form of the time-dependent Green function as follow

$$K(x,x_0,t) = \frac{a(xx_0)^{\frac{1}{2}}}{4\pi^2}\int_0^{\infty} \alpha e^{\frac{-a^2\alpha^2}{8}t}\sinh(\pi\alpha)\left|\Gamma(i\alpha)\right|^2 \times W_{\frac{1}{2},\frac{i\alpha}{2}}(\frac{1}{x_0})W_{\frac{1}{2},\frac{i\alpha}{2}}(\frac{1}{x})d\alpha. \tag{39}$$